

Modelling, simulation and experimental tests for process scaling of cutting processes with geometrically defined edge

J. Kotschenreuther¹, L. Delonnoy², T. Hochrainer³, J. Schmidt¹, J. Fleischer¹, V. Schulze², D. Löhé², P. Gumbsch³

¹Institute of Machine Tools and Production Science, Karlsruhe

²Institute of Materials Science and Engineering I, Karlsruhe

³Institute for Reliability of Systems and Devices, Karlsruhe

Abstract

Experimental cutting studies and Finite Element Method (FEM)-based studies were performed to investigate size effects occurring in micro-cutting of steels. In a dry turning process a high precision Kugler MicroMaster 2 was used to measure cutting forces and roughness of specimens made of S235-steel. In the FEM-studies a material routine based on a plasticity model for high speed deformation was implemented in ABAQUS. A dimensional analysis of the material model used was performed and during application in the single shot impact problem similarity relations were derived. It was started to transfer this strategy to micro-cutting.

1 Introduction

One main tendency in technology is the miniaturization of devices and components. Micro-fluidic, micro-mechanic, micro-optic and micro-electronic devices are combined as micro-systems allowing for new products. For a major breakthrough of micro-technology an economical processing is of vital importance. At the present time most manufacturing processes are adapted from the semi-conductors industry, which are only economical for very large lots. Furthermore these processes which are usually lithographic strongly restrict the design geometry. Micro-cutting has the potential to overcome these problems and to offer new fields of application to micro-technology.

When the cutting-depth decreases to the order of micro-meters some unexpected phenomena appear which for example concern the needed cutting force or the quality of the machined surface. These phenomena, not foreseen by conventional scaling used for dimensioning in cutting technology, are summed up as so called size-effects.

The goal of this joint research project is a deeper understanding of these size effects, aiming on the enhancement of the technical practicability of micro-cutting. Main tool for this is a combination of finite element simulations with the methods of similarity mechanics in order to clarify the vital input parameters and describe their influence in terms of similarity relations. Because of the high complexity of the cutting process and the time consumption for its simulation, we first showed the capabilities of this procedure at the model problem of single shot impact, which may also be seen as a part of a shot peening process.

The theoretical investigations of course have to be compared to experimental results. An experimental setup for micro cutting has been developed using a Kugler MicroMaster 2. First tests have been carried out using a preliminary workpiece material S235 in a dry turning process.

2 Setup

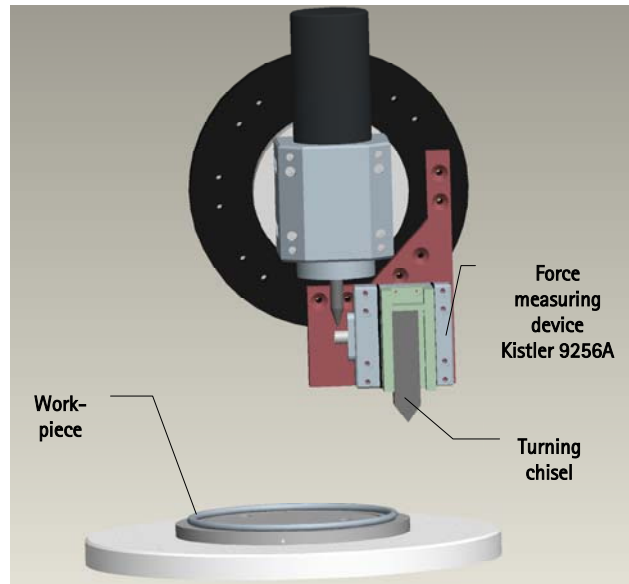


Fig. 1: View of experimental layout on the Kugler MicroMaster 2

2.1 Tools and cutting materials

The chisel is a standard item to accept indexable inserts CCMW 12 04 08 with a neutral angle of inclination. The tested tool materials are TiN-coated cemented carbide inserts as well as Saphir-like Al_2O_3 inserts, which show a cutting edge radius of about $10\ \mu\text{m}$ in case of the cemented carbide and $1\text{-}2\ \mu\text{m}$ in the case of Al_2O_3 . Geometries of the cutting tools were in both cases rake angle $\gamma = 0^\circ$ as well as clearance angle $\alpha = 7^\circ$.

2.2 Process parameters

The cutting speed was varied in a turning process in which the ring shaped workpiece (inner diameter 150 mm and outer diameter 156 mm) was rotating at 100, 200 and 400 rpm. Together with the mean radius of the ring, the cuttings speeds were 48.5 m/min, 97 m/min and 194 m/min. The process was divided into three parts starting with an increasing depth of cut thus creating a slope, followed by a component of constant depth of cut whereas the last phase featured a decreasing depth of cut, thus creating another slope. During these variations the chisel was also moved in the direction of the workpiece center point in order to obtain arbitrary tool path lengths, thus creating a coil-shaped groove. The depth of cut has been varied between $100\ \mu\text{m}$ and $10\ \mu\text{m}$.

2.3 Measurements

The cutting forces were measured using a force measuring device Kistler 9256A2 (range of operation: -250 N ...250 N, response threshold <0.002 N, eigenfrequencies $f_0(x) \sim 4.0$ kHz, $f_0(y) \sim 4.8$ kHz, $f_0(z) \sim 4.6$ kHz) and the surface roughness values were measured using a confocal white light microscope of type Nanofocus.

3 Experimental Results

3.1 Cutting force

The size effect in metal cutting is commonly known as the increase in the cutting force per unit depth of cut with a decrease in the depth of cut.

The absolute and the specific cutting forces observed during the experiments were as following from Fig.2.

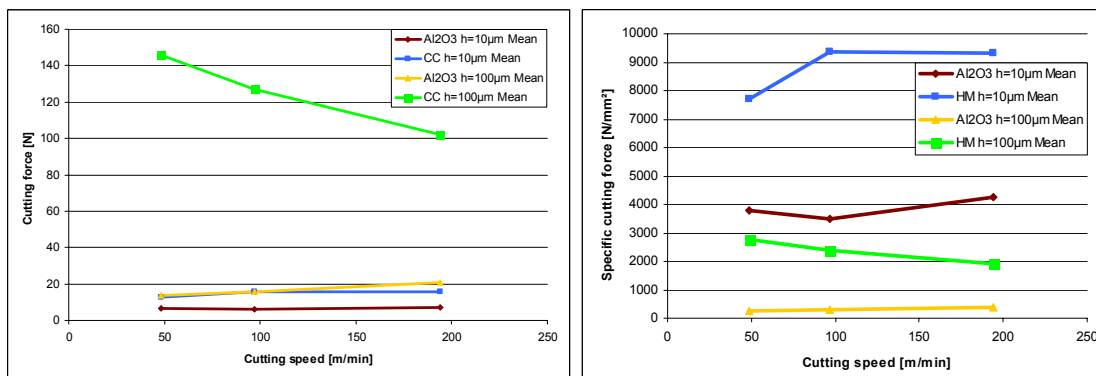


Fig. 2: Cutting force vs. cutting speed and specific cutting forces vs. cutting speed

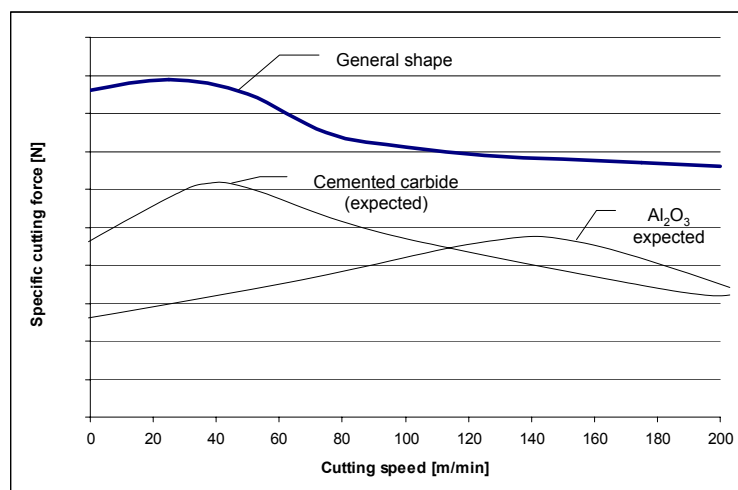


Fig. 3: Specific cutting force vs. cutting speed according to Vieregge (schematically) [1]

Fig. 2 indicates, that the cemented carbide tool with a cutting edge radius of 10 µm seems to have passed the cutting force climax at the highest cutting speed. In contrast, Al₂O₃ with a cutting edge radius of 1 µm has not yet reached it. The expected curves of cemented carbide and Al₂O₃

depicted in Fig. 3, were created based on the results shown in Fig.2 (right hand side). This is subject to further research insofar that cutting speeds lower and higher than the actual values are required to verify the actual position of the maxima in Fig. 3. Based on the current layout of the workpiece i.e. diameter of 156 mm and the limitations of the c-axis of the machine, higher cutting speeds could not be achieved, this task will be engaged in the further scope of the experiments by increasing the radius of the workpiece.

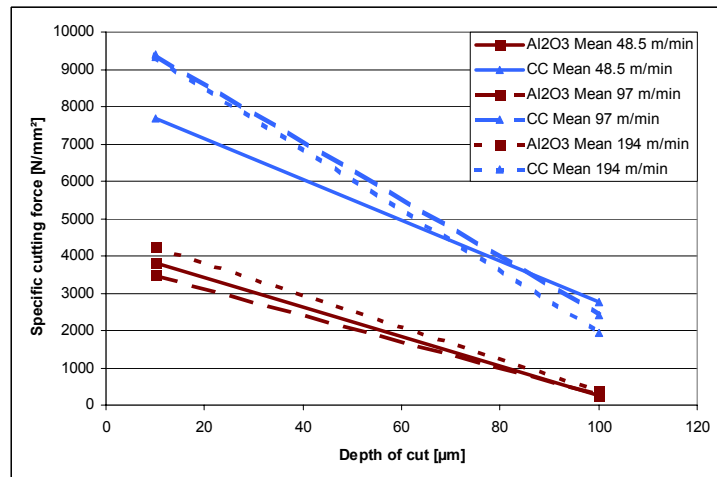


Fig. 4: Specific cutting force vs. depth of cut

Altan [2] found by simulation that an increasing edge radius leads to an increasing chip thickness and a decreasing shear angle. Due to the reduced shear angle and the increased chip thickness there is a larger shear plane in the deformation zone, which increases the cutting forces. In addition, the increased radius leads to an increase in the ploughing force which again leads to increasing cutting forces. Altan varied the cutting edge radii between 10 μm to 100 μm as well as the depth of cut between 600 μm to 700 μm . The presented results show that this still is true for smaller cutting edge radii and depth of cut.

Fig. 4 illustrates the experienced result of the size effect namely, that the specific cutting force rises as expected with decreasing depth of cut. Experimental results obtained by Kim et al. [3] confirmed that the cutting force increases as the tool edge radius increases. These tendencies can also be observed in Fig. 4 for Al₂O₃ with the cutting edge radius of 1 μm and cemented carbide with the cutting edge radius of 10 μm .

3.2 Roughness

Roughness was measured parallel to the cutting direction in order to receive information on the cutting process.

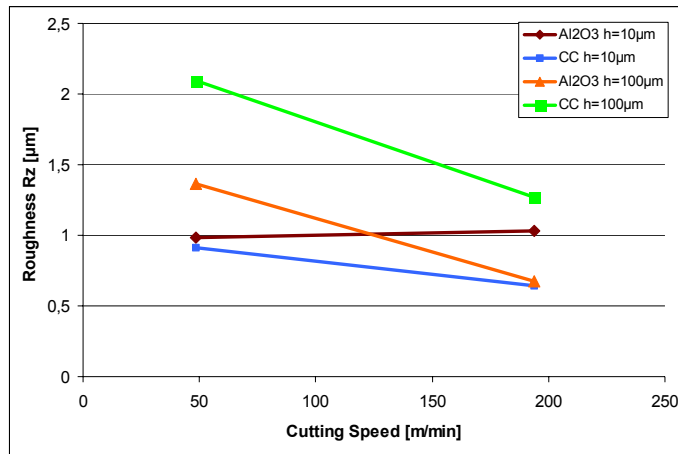


Fig. 5: Roughness R_z of S235 measured parallel to cutting direction [4]

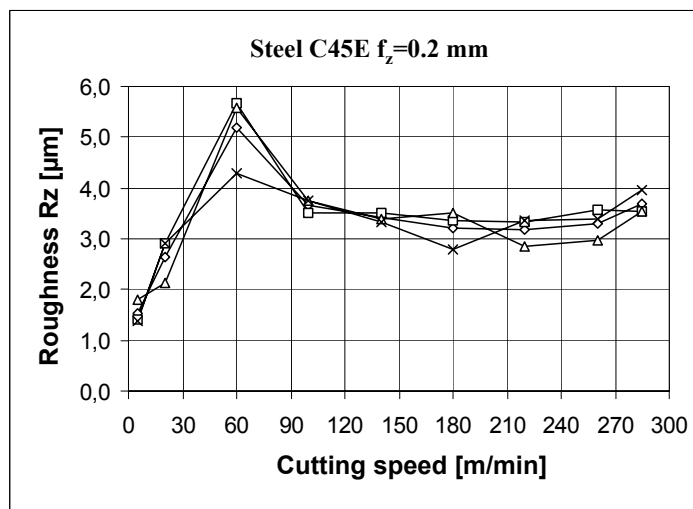


Fig. 6: Roughness R_z vs. cutting speed in a milling process

Fig. 5 illustrates that the roughness at higher depth of cuts tend to be more affect the cutting speed than lower ones for larger cutting edge radii. In contrast to this the influence of cutting depth does not seem to be given for the smaller cutting edge radius. An overall reduction of roughness with increasing cutting speed can be observed, which corresponds well with existing models. However it is interesting that the roughness of cemented carbide with a cutting depth of $h = 10 \mu\text{m}$ is below the ones of Al_2O_3 . It needs to be clarified whether this can be related to an effect (e.g. build-up edge) or be declared as scattering.

Comparing Fig. 5 and Fig. 6 it can be seen that the obtained values in Fig.5 fit into the slope after 60m/min in Fig. 6 which were obtained at the wbk while micro milling steel C45E. This curve however holds true for turning too and is a commonly known fact. Further variation in the cutting speed will help to compare the results of Fig. 6 with those of measured after turning of S235.

Thiele and Melkote [5] also observed an increasing edge radius tending to increase the average surface roughness due to the increase in the ploughing force.

4 Material Model and VUMAT

For the simulation of the process of chip formation the modeling of the materials behavior at high strain rates, including a thermo-mechanical coupling and a reasonable separation criterion plays a vital role. In order to implement the appropriate materials behavior into the commercial FEM package ABAQUS/Explicit, a user subroutine VUMAT was developed. This will be outlined at the end of this section after presenting the material model.

The basis for the elasto-plastic behavior is the yield stress σ_y depending on temperature T and strain rate $\dot{\epsilon}$ based on the idea of thermally activated overcoming of short range obstacles by dislocations as proposed in [6]. Introducing the scalar total dislocation density ρ thus the yield stress

$$\sigma_y = \sigma_G(\rho) + \sigma^*(T, \dot{\epsilon})$$

can be additively split into an athermal (only temperature dependent proportional to the temperature dependence of the elastic moduli) part $\sigma_G(\rho)$ with strain hardening and a thermal part $\sigma^*(T, \dot{\epsilon})$, which is temperature and strain rate dependent, but independent of strain at bcc materials like the steels investigated.

In the VUMAT the first part is modeled by a rather simple power law for strain hardening as proposed by Holomon.

The second part is derived from an Arrhenius law for the thermally activated overcoming of short range obstacles which leads to

$$\sigma^*(T, \dot{\epsilon}) = \sigma_0^* \left(1 - \left(\frac{T}{T_0} \right)^n \right)^m$$

where

$$T_0 = \frac{\Delta G_0}{k \ln \frac{\dot{\epsilon}_0}{\dot{\epsilon}}}$$

is a strain rate dependent critical temperature. As further material parameters the free activation enthalpy necessary to overcome the decisive short range obstacles ΔG_0 , a critical strain rate $\dot{\epsilon}_0$ which is determined by the density of glide dislocations, their Burgers vector, the Debye frequency and the Taylor factor, and the thermal part of the yield stress at zero Kelvin σ_0^* are introduced. Furthermore the exponents n and m describe the shape of the obstacles. As usual k denotes the Boltzmann constant. For the cutting simulation additionally a failure criterion of Johnson and Cook [7] was included, making the failure dependent on the multiaxiality of the stress state, the temperature and the strain rate. Let ϵ_f denote the equivalent plastic strain at failure, then this has the form

$$\varepsilon_f = \left(d_1 + d_2 \exp\left(d_3 \frac{\rho}{\bar{\sigma}} \right) \right) \left(1 + d_4 \ln \dot{\varepsilon} \right) \left(1 + d_5 \frac{T - T_{room}}{T_{melt} - T_{room}} \right),$$

where $\rho = \frac{1}{3} \sigma_{ii}$, $\bar{\sigma}$ is the von Mises equivalent stress, T_{melt} and T_{room} are melting and room temperature and the coefficients d_1, \dots, d_5 are material parameters. For further details it is referred to the original work of Johnson and Cook [7].

As isotropic plastic behavior is assumed, the von Mises yield function given in short as

$$F(\sigma) = \bar{\sigma} - \sigma_y$$

is applied. In the VUMAT the according one-dimensional differential equation for plastic yield is integrated implicitly by solving for the equivalent plastic strain rate $\dot{\varepsilon}_p$ in the equation

$$F(\sigma + \Delta t \dot{\sigma}(\dot{\varepsilon}_p), \varepsilon_p + \Delta t \dot{\varepsilon}_p, \dot{\varepsilon}_p, T + \Delta t \dot{T}(\dot{\varepsilon}_p)) = 0$$

using a Newton-Raphson method.

Two versions of the VUMAT, one providing the thermo-mechanical coupling via locally adiabatic heating, treating temperature as an inner variable, and one providing the information needed by ABAQUS for a full thermo-mechanical coupling including thermal expansion, heat transfer were implemented.

5 Development of extended similarity relations at single shot impacts

In the miniaturisation of cutting processes size effects result for example from not uniformly scalable process variables (as e.g. relation of cutting edge radius to the thickness of cut) or not uniformly scalable microstructure parameters (grain size, dislocation density). Similarity mechanics are used to determine size effects and to transfer results to other process conditions. In order to show the practicability of the similarity mechanics method single shot impacts were simulated in preliminary studies, which may give also informations on size effects in shot-peening.

5.1 Model geometry

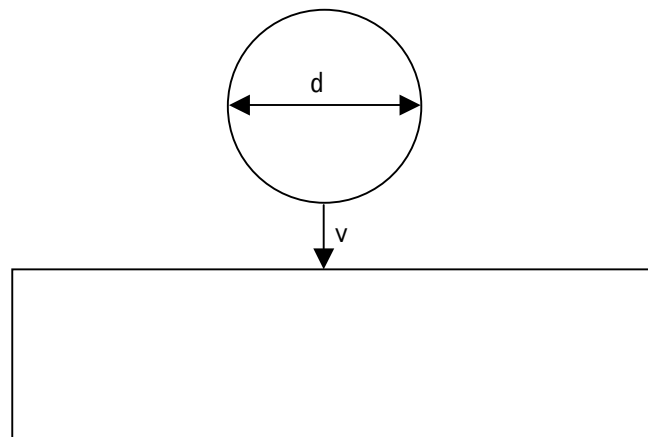


Fig.5: Model of single shot impact

The sphere with a diameter d hits the plate with impact speed v . In order to keep the number of elements as small as possible and thus the computing time, the sphere and the plate are simplified and modelled in an idealized manner. Therefore, a fine cross-linking of the plate was necessary in the zone, where the sphere affects the plate. Fig. 6 shows the model of single shot impact used in the simulations.

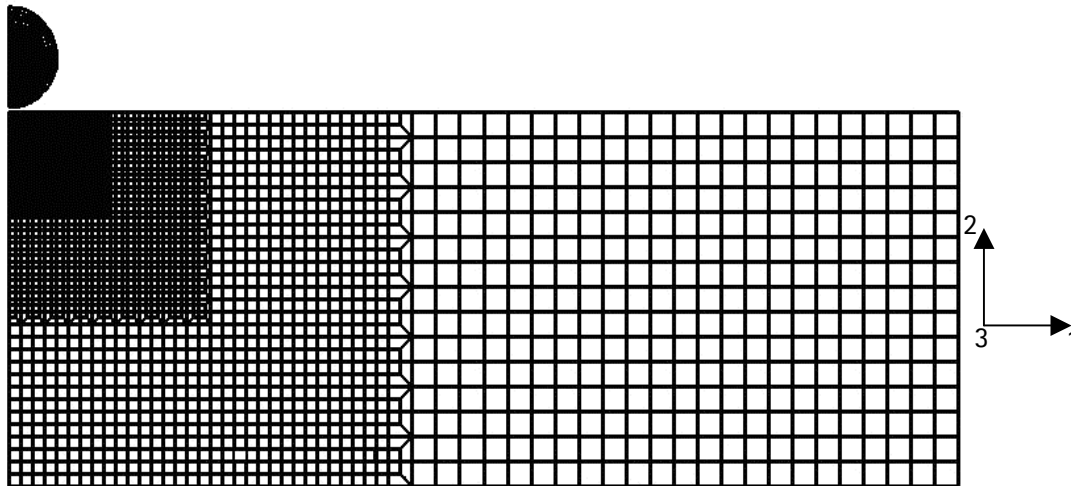


Fig. 6: Mesh of single shot impact used in simulation

The workpiece is elasto-plastic with strain rate and temperature dependent materials behavior. Table 1 shows standard material indices of normalized C45E. The sphere is assumed to be purely thermoelastic showing the same thermoelastic properties as the plate.

standard material parameters	C45E (plate)
Density ρ [g/cm^3]	7,8
modulus of elasticity E [MPa]	$2,1 \cdot 10^5$
Poisson's ratio ν	0,28
Hardening coefficient h [MPa]	435
Microstructure coefficient σ_0 [MPa]	330
thermal yield stress coefficient σ_0^* [MPa]	2000
Strain rate coefficient $\dot{\epsilon}_0$ [s^{-1}]	$4,41 \cdot 10^7$
Activation enthalpy ΔG_0 [J]	$1,02528 \cdot 10^{-19}$
Specific thermal capacity c_p [$\text{J} \cdot \text{kg}^{-1} \cdot \text{K}^{-1}$]	460
Conductivity λ [$\text{W} \cdot \text{m}^{-1} \cdot \text{K}^{-1}$]	50
Thermal expansion α [K^{-1}]	$11,5 \cdot 10^{-6}$

Tab. 1: Material parameters for Ck45 standard material [8]

Friction between sphere and plate neglected. The standard impact conditions are assumed as follows:

diameter of shot $d = 0,2 \text{ mm}$

impact speed $v = 25 \text{ m.s}^{-1}$

initial temperature of shot $T_{i1} = 293 \text{ K}$

initial temperature of plate $T_{i2} = 293 \text{ K}$

The simulation is calculated with the VUMAT with full thermo-mechanical coupling including thermal expansion, heat transfer in Abaqus \ Explicit.

5.2 Results of simulation

Fig. 7 exemplarily shows the simulation results of displacement of the plate surface in z-direction after the shot impact.

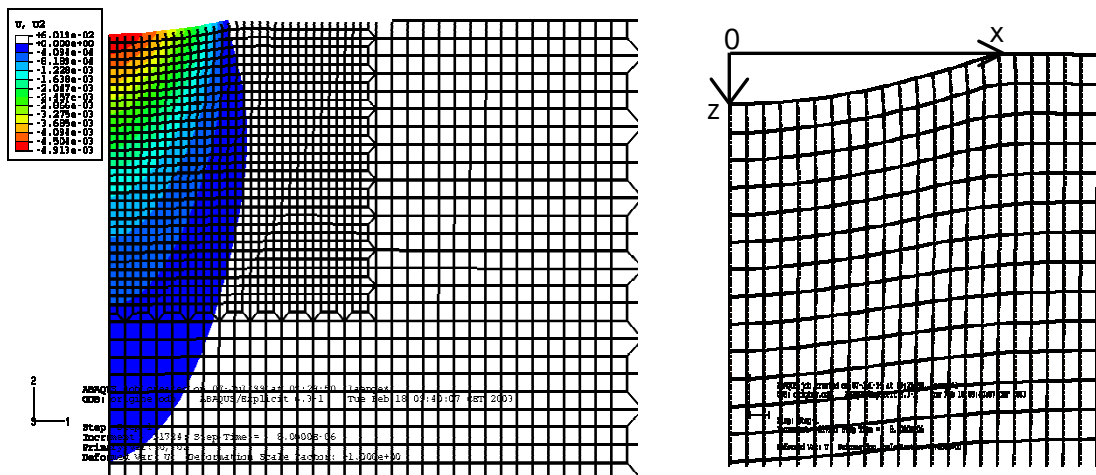


Fig. 7: Displacement of the plate surface in z-direction after the single shot impact

The value of interest thereafter is a dimensionless output value. For example the following ratio z/d will be chosen here, which has a standard value of:

$$\left(\frac{z}{d} \right)_o = 0,2455$$

5.3 Similarity mechanics

According to the Buckingham theorem, a dimensionless output value a of a physical problem depends only on $p = n - q$ dimensionless numbers D_1, \dots, D_m , whereby n is the number of influence parameters and q is the rank of the dimension matrix. Table 2 shows the dimension matrix of the single shot impact, where the index p addresses the plate and s addresses the sphere.

Influence parameters Fundamental units	d	v	T_{a,p,s}	E_{p,s}	ρ_{p,s}	σ_G	h	σ₀[*]	T_c = $\frac{\Delta G_0}{k_B}$	ε̇₀	c_{p,p,s}	α_{p,s}	λ_{p,s}
Length	1	1		-1	-3	-1	-1	-1			2		1
Time		-1		-2		-2	-2	-2		-1	-2		-3
Mass				1	1	1	1	1					1
Temperature			1						1		-1	-1	-1

Tab. 2: Dimension matrix for the single shot impact

That means that to fully describe the scaling problem of the impact, it is necessary to find 15 dimensionless numbers ($p = 19 - 4$). The knowledge of the functional dependencies of a dimensionless output a on the 15 numbers $a = a(D_1, \dots, D_{15})$ would then completely describe the scaling here.

The choice of the dimensionless numbers is done in a way that whenever possible, each varying input parameter only affects a single number. As can be seen below the velocity for example only affects the so called Cauchy number, giving the ratio of the impact velocity to the internal sound velocity of the plate.

The 15 dimensionless characteristic numbers were grouped according to the input parameters used to vary then as follows:

1. Process parameters

Size	rate	Temperature
$Si = \frac{\dot{\epsilon}_0 \cdot d}{\sqrt{E/\rho}}$	$Ca = \frac{v}{\sqrt{E/\rho}}$	$Te = \frac{T_i}{T_c}$

2. Elasto-plastic material parameters

microstructure	Hardening	thermal yield stress	specific thermal capacity	thermal expansion	thermal conduction
$Mi = \frac{\sigma_G}{E}$	$H = \frac{h}{E}$	$Th = \frac{\sigma_0^*}{E}$	$TCa = \frac{\rho \cdot c_p \cdot T_c}{E}$	$TE = \frac{E \cdot \alpha}{\rho \cdot c_p}$	$TCo = \frac{\lambda \cdot \dot{\epsilon}_0}{E \cdot c_p}$

3. Ratio numbers

ratio of Young`s moduli	ratio of density	ratio of initial temperature
E_{sphere} / E_{plate}	$\rho_{sphere} / \rho_{plate}$	$T_{i,sphere} / T_{i,plate}$
ratio of specific thermal capacity	ratio of thermal expansion coefficient	ratio of thermal conductivity
$c_{\rho,sphere} / c_{\rho,plate}$	$\alpha_{sphere} / \alpha_{plate}$	$\lambda_{sphere} / \lambda_{plate}$

From the Buckingham theorem it is clear that if all similarity numbers remain constant, i.e. coordinated change of process variables and material parameters, all dimensionless output values must remain constant, too.

A check, ensuring that a complete set of dimensionless numbers for this problem was found, was performed as follows. The diameter d was varied and the material parameters were adjusted such, that all numbers remained constant. It can be seen from Fig. 8 that the dimensionless output value z/d remains constant with increasing diameter. The same could be shown for all other dimensionless output values.

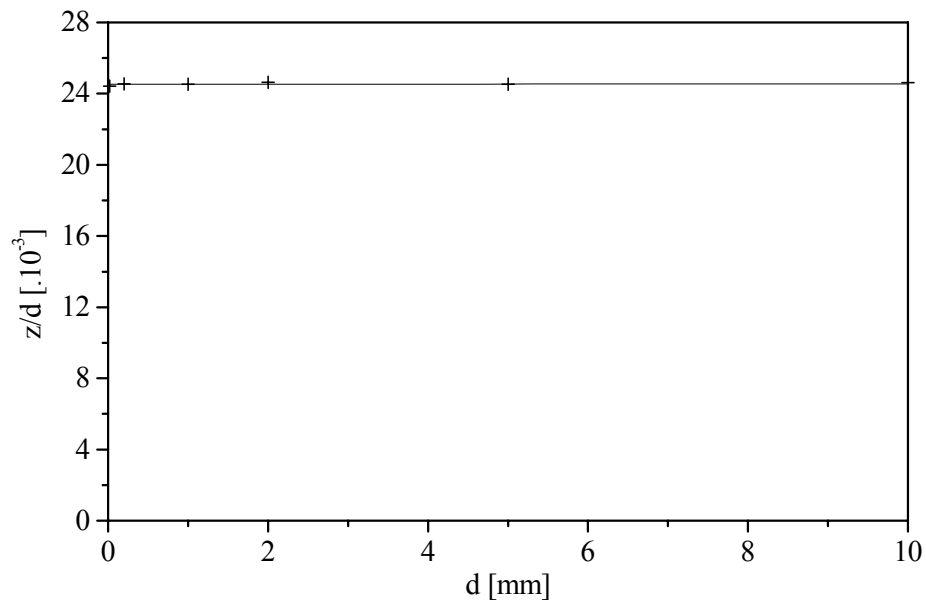


Fig. 8: Dependence of the dimensionless output value z/d on the sphere diameter d

5.4 Application of the results

The similarity mechanics should be used for the prediction of output values for other process conditions or materials. Using the Buckingham theorem, the number of influence factors could

already be reduced from 19 influence parameters to 15 dimensionless characteristic numbers, which in fact still is far too much.

Therefore the parameters, which may vary, were reduced and as further simplification, a product ansatz, stating

$$a(D_1, \dots, D_p) = K \cdot a_1(D_1) \cdot \dots \cdot a_p(D_p)$$

was made. Here $K = \frac{1}{a_o^{p-1}}$, $p = \#(\text{similarity numbers})$

and a_o represent the output value for standard material parameters and standard process parameters as given in Section 5.1.

As an example, for the impact problem, a fixed material with constant initial temperature was selected. That means that only diameter (Si) and velocity (Ca) may vary. The process variable vary as $0,02 < d < 10 \text{ mm}$ and $0,25 < v < 50 \text{ m/s}$. The product ansatz gives here the following form:

$$\frac{z}{d} = K \cdot \frac{z}{d}(Si) \cdot \frac{z}{d}(Ca) \quad \text{with} \quad K = \frac{1}{\left(\frac{z}{d}\right)_o^{2-1}}$$

The dependencies of the dimensionless output value z/d on the dimensionless numbers Si and Ca are shown in Fig. 9. Additionally, mathematic descriptions of these dependencies are given there.

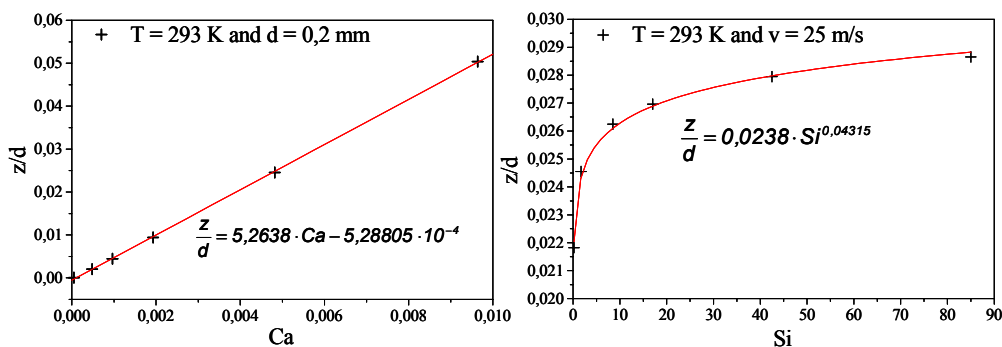


Fig. 9: Dependence of the dimensionless output value z/d on the dimensionless numbers Ca and Si

As an example for the predictions with the product ansatz for the output value z/d the predictions for a sphere diameter $d = 0,56 \text{ mm}$ and a velocity $v = 35 \text{ m.s}^{-1}$ were compared with the result of the simulation. The results are:

$$\frac{z}{d}(d = 0,56 \text{ mm}, v = 35 \text{ m/s})_{simulation} = 0.03675$$

$$\frac{z}{d}(d = 0,56 \text{ mm}, v = 35 \text{ m/s})_{product} = 0.03630$$

This is a relative error of approximately 1.3 %, showing a very good applicability of the product ansatz.

The product ansatz was also successfully checked for three varying parameters. Thus it is possible to predict various output values for different materials and process conditions after doing a reasonably low number of simulations.

6 Similarity mechanics for a 2D turning process

The similarity mechanics for the cutting process is quite similar to that of the impact problem described above, as the same material models are applied. This means, that the workpiece was modelled using the elasto-plastic material model (VUMAT) formerly used for the plate and the tool as (thermo-) elastic like formerly the sphere. The only differences thus arise from the different geometry, kinematics and the separation criterion not included in the single shot impact. Starting with the geometry, an idealized two dimensional model of a turning process can be described completely by defining:

1. chipping thickness h
2. cutting edge radius r
3. rake angle γ
4. clearance angle α

Further parameters needed to describe the geometry of tool and workpiece are assumed to have no influence, as long as the workpiece dimensions are big compared to the chipping thickness h . Lateral effects as the width of the cut should be studied later as these will need 3D simulations.

The kinematics is again completely characterized by a velocity, which is the cutting speed here. A

5. cutting speed v

can be prescribed rather than a cutting force F_c , which is one of our main output parameters. Again, additionally a

6. starting temperature T_i of workpiece and tool, which are always taken as equal,

has to be given. According to the grouping of the dimensionless numbers via process variables, elasto-plastic material parameters and ratio numbers, only a change in the first group occurs, except for interchanging sphere and plate with tool and workpiece respectively and introducing the friction coefficient η as another dimensionless number in the third group. For completeness a fourth group for the failure criterion is introduced. This introduces five additional dimensionless numbers D_1, \dots, D_5 which are but taken as constant and thus neglected in the following.

The first group then is:

chipping thickness	velocity	Temperature	Ratio of edge radius to chipping thickness	Rake angle	clearance angle
$Si = \frac{\dot{\epsilon}_0 \cdot d}{\sqrt{E/\rho}}$	$Ca = \frac{v}{\sqrt{E/\rho}}$	$Te = \frac{T_i}{T_c}$	$\frac{r}{d}$	γ	α

7 Simulation of the cutting process

The two dimensional geometry and the mesh were built with ABAQUS/CAE. An infinitely sharp cutting tool was assumed and the first calculation was performed applying a slightly negative rake angle $\gamma = -3^\circ$ and a clearance angle $\alpha = 3^\circ$. The model definition incorporates two important features. The first is, that a much coarser mesh in the bulk of the workpiece than in the region likely to form the chip could be achieved by using the option *Tie to enforce ABAQUS to treat it as one body only, see Fig. 10.

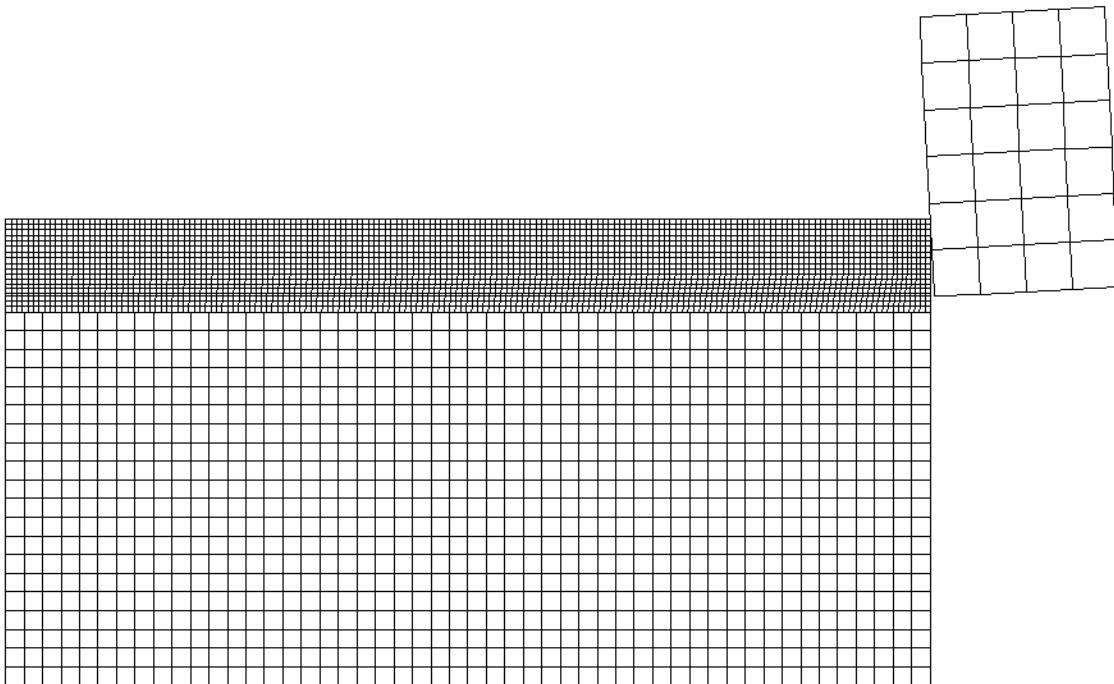


Fig. 10: Geometry used for the cutting simulation

The second point is that the internal remeshing algorithm "ALE" from ABAQUS is used in the chip, which prevents the elements from becoming too much distorted and unfavorably shaped. As the remeshing algorithm terminates when elements become excessively distorted although they were previously "deleted" by the VUMAT, it unfortunately has to be ensured that in the remeshing zone no element deletion (failure) occurs. The usage of the Johnson and Cook failure criterion, explained in the section on the material model, showed that with our material model no failure occurs in the primary shear zone, due to the high pressure. In order to detect the cutting path it is thus enough to enable failure only for a small region above and everywhere below the theoretical cutting path, prescribed by the kinematics of the tool. In Fig. 11 the ALE-Zone, where no failure is allowed, is highlighted.

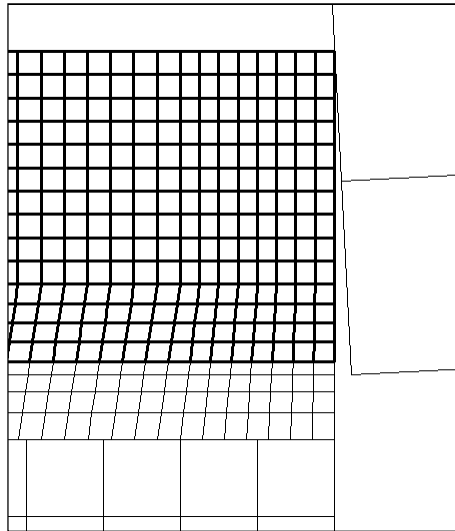


Fig. 11: ALE-Zone at the start in the vicinity of the tool tip. In this zone no element deletion is allowed

The current simulations are preliminary in two ways, as the actual experimental geometry and cutting speed are not finally fixed and moreover the tool steel 90MnCrV8 which will be used later as workpiece material is not yet characterized. Thus a rather theoretical geometry and the materials parameters of Ck45 are used, known from a former work on high speed cutting. Until now only a small set of calculations was made analyzing the influence of the cutting speed on the cutting force. Thereby the following parameters were applied:

$$h = 8 \mu\text{m}, r = 0, \gamma = -3^\circ, \alpha = 3^\circ, T_a = 293^\circ\text{K}$$

The cutting force was used for 4 velocities, namely 200, 600, 1200 and 2000 m/min, using the VUMAT which allows for full thermo mechanical coupling (Fig.12).

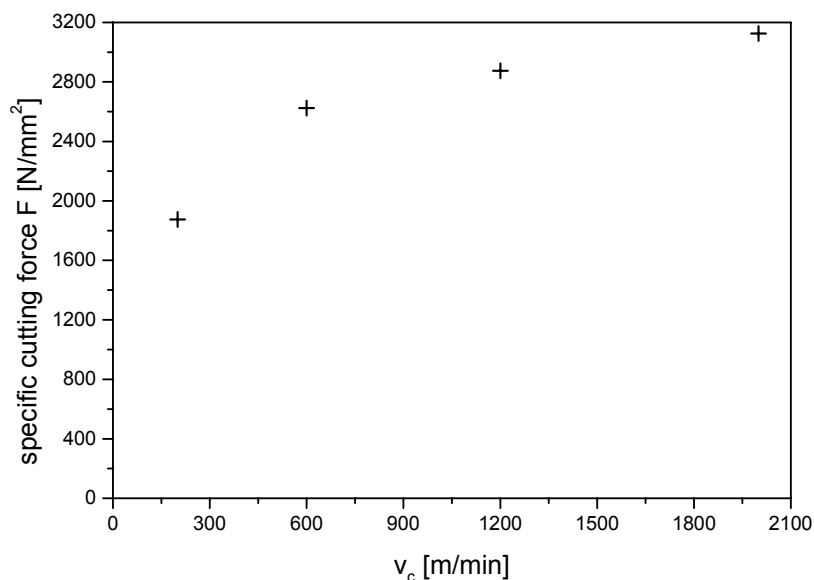


Fig. 12: Specific cutting force vs. cutting speed at $h=0.008$ mm

A direct comparison to the experimental data shown in Section 3.1 is not of much evidence, because of the problems with different materials, geometries and cutting speeds as explained above. So at the moment it can just be stated, that the simulation is giving specific cutting forces of the right order of magnitude.

8 Summary

Experimental cutting studies and Finite Element Method (FEM)-based studies were performed to investigate size effects occurring in micro-cutting of steels. In a dry turning process a high precision Kugler MicroMaster 2 was used to measure cutting forces and roughness of specimens made of S235-steel. In the FEM-studies a material routine based on a plasticity model for high strain rate deformation was presented, which is implemented in ABAQUS. A complete dimensional analysis was carried out and the method of combining similarity mechanics with FEM simulations was shown to be powerful for predicting the scaling of processes at the model problem of single shot impact.

The next phase will deal with experiments and simulations with the workpiece materials 90MnCrV8 and Armco-Iron, which is a model material with an extremely low content of carbon. Different states of these materials regarding heat treatments, grain size, carbon contents and mechanical properties, will be considered.

9 References

- [1] Vieregge, G, 1959, "Zerspanung der Eisenwerkstoffe", Stahleisenbücher, p.47
- [2] Yen, E., Jain, A., Altan, T., 2002, "A Finite Element Analysis of Orthogonal Machining using Different Tool Edge Geometries" submitted to the *Special Issue of JMPT*
- [3] Kim, K.W., Lee, W.Y. and Sin, H.C., 1999, *Journal of Materials Processing Technology*, Vol. 86, pp. 45-55
- [4] Hüntrup, V., 2000, "Untersuchungen zur Mikrostrukturierbarkeit von Stählen durch das Fertigungsverfahren Fräsen", Institute of Machine Tools and Production Science, University Karlsruhe, p. 87
- [5] Thiele, J.D. and Melkote, S.N., 1999, *Journal of Materials Processing technology*, Vol. 94, pp. 216-226
- [6] Burgahn F., Schulze V., Vöhringer O., Macherauch E., *Mat.-wiss., u. Werkstofftech.* 27, 521-530 (1996)
- [7] Johnson G. R., Cook W. H., *Engineering Fracture Mechanics* 21 (1), 31-48 (1984)
- [8] Biesinger F., Söhner J., Schulze V., Vöhringer O., Weule H., 2000, Simulation des Spanbildungsprozesses beim Hochgeschwindigkeitsfräsen, Institute of Materials Science and Engineering I, University Karlsruhe, Report within DFG-SPP „Spanen metallischer Werkstoffe bei hohen Geschwindigkeiten“